Review Article

Journal of Environmental Nanotechnology

A Comparative Simulation Study of Modified Incremental Conductance and Perturb-and-observe Algorithms for Enhanced Efficiency under Dynamic Environmental Conditions

P. Vinod Kumar[1*], Dr. K. Sakthivel[1] and A. Nagamani Prabu[2]

[1]Department of Electrical and Electronics Engineering, Bharth Institute of Higher Education and Research, Chennai, TN, India
[2]Department of Physics, Karpagam Academy of Higher Education, Coimbatore, TN, India
Received: 15.01.2026 Accepted: 25.02.2026 Published: 30.03.2026
*p.v.kumardev@gmail.com

ABSTRACT

This study presents a nanomaterial-engineered solar energy conversion and storage system that integrates a quasi-Z-source converter with adaptive maximum power point tracking (MPPT) algorithms, namely Modified Incremental Conductance (MIC) and Modified Perturb-and-Observe (M-P & O), to enhance photovoltaic (PV) performance under dynamic irradiance conditions. The overall system behaviour and control effectiveness are systematically evaluated using MATLAB/Simulink-based simulations. Simulation results demonstrated that the MIC algorithm offers superior voltage stability, faster dynamic response, and higher tracking accuracy compared to the M-P & O approach. It achieved 1.6 kW additional simulated power output at a standard operating temperature of 25 °C. The proposed PV module employed a hybrid nanomaterial configuration in which quantum dots and graphene derivatives are embedded within the photoactive layer to broaden spectral absorption and improve charge carrier mobility, while metal oxide nanoparticles such as TiO_2 and ZnO enhance interfacial charge separation and suppressed the recombination losses. These nanomaterial-induced modifications result in nonlinear and dynamically varying current–voltage characteristics, thereby necessitating adaptive MPPT control. The dynamic step-size adjustment mechanism implemented in the MIC algorithm effectively accommodated these variations, enabling stable and efficient energy extraction. Overall, simulation-based findings indicate an efficiency improvement of approximately 6–8%, demonstrating a scalable and sustainable pathway for high-performance solar energy systems.

Keywords: Nanomaterial-based photovoltaic systems; Quasi-Z source converter; Modified incremental conductance algorithm; Modified perturb and observe algorithm; Solar photovoltaic system.

1. INTRODUCTION

Maximum Power Point Tracking (MPPT) plays a central role in maximizing the energy yield of photovoltaic (PV) systems by continuously regulating the operating point under varying environmental and electrical conditions (Esram and Chapman, 2007; Reisi *et al*. 2013). Among the numerous MPPT strategies proposed in the literature, Perturb-and-Observe (P&O) and Incremental Conductance (INC) remain the most widely adopted due to their relative maturity, ease of implementation, and adaptability across diverse PV configurations (Hohm and Ropp, 2003; Femia *et al*. 2005). Both algorithms aim to locate the maximum power point (MPP) by exploiting the nonlinear characteristics of PV modules; however, their tracking performance is strongly influenced by irradiance fluctuations, temperature variations, and partial shading phenomena (Walker, 2001; Safari and Mekhilef, 2011). Under rapidly changing operating conditions, conventional P&O methods may experience delayed convergence and persistent oscillations around the MPP, whereas INC-based approaches exhibit improved responsiveness by explicitly evaluating the slope of the power- voltage relationship (Esram and Chapman, 2007). These distinctions have been consistently documented under transient environmental scenarios rather than under steady-state operation, where both algorithms demonstrate comparable performance (Hohm and Ropp, 2003).

Recent developments have focused on enhancing the INC algorithm through adaptive control mechanisms to mitigate its sensitivity to noise and computational overhead (Femia *et al.* 2005; Reisi *et al.* 2013). Modified INC schemes improve tracking precision primarily during fast irradiance transitions and irregular shading events by dynamically adjusting step sizes and convergence criteria (Safari and Mekhilef, 2011). In contrast, the P&O algorithm continues to be favored in applications where environmental conditions are relatively stable and controller simplicity is prioritized (Walker, 2001). Thus, rather than a universal superiority, the performance distinction between P&O and INC is dependent upon operating dynamics, system complexity, and control responsiveness (Esram and

Chapman, 2007). Recognizing these contextual dependencies is essential for aligning MPPT strategies with emerging PV technologies.

In parallel with advances in control algorithms, nanomaterial integration has emerged as a transformative pathway for improving PV performance at the material level (Atwater and Polman, 2010; Green *et al.* 2014). Nanostructured components including quantum dots, graphene-based derivatives, carbon nanotubes, and metal oxide nanoparticles modify light-matter interactions by enhancing spectral absorption, improving charge carrier transport, and reducing recombination losses (Snaith, 2013; Nozik, 2010). These material-level enhancements significantly alter the electrical behavior of PV modules, resulting in more complex and dynamically varying current-voltage (I–V) and power-voltage (P–V) characteristics under changing irradiance and temperature conditions (Green *et al.* 2014). Consequently, the incorporation of nanomaterials does not merely improve conversion efficiency but also introduces new control challenges for MPPT algorithms, which must respond to steeper curve gradients, localized extrema, and rapid parameter variations (Atwater and Polman, 2010).

This intrinsic coupling between nanomaterial-induced electrical dynamics and MPPT performance necessitates a shift toward more adaptive and analytically grounded tracking techniques (Nozik, 2010). Nanomaterial-engineered PV surfaces exhibit increased sensitivity to spectral and thermal fluctuations, which can amplify the limitations of conventional perturbative methods such as P&O (Safari and Mekhilef, 2011). In contrast, INC-based approaches, particularly those capable of estimating instantaneous slope variations are better suited to accommodate the nonlinear and time-varying behavior introduced by nanoscale modifications (Reisi *et al.* 2013). Therefore, the relevance of advanced INC variants is not rooted in generalized efficiency claims but in their structural compatibility with the evolving electrical signatures of nanomaterial-enhanced PV systems (Femia *et al.* 2005).

Despite these advancements, existing studies frequently treat nanomaterial innovation and MPPT control design as isolated domains, resulting in fragmented optimization strategies (Green *et al.* 2014). A cohesive framework that integrates material-level enhancements with control-level adaptability remains insufficiently explored (Atwater and Polman, 2010). Moreover, comparative analyses of P&O and INC algorithms are often presented independently of the altered operating landscapes created by nanostructured PV materials, limiting their practical relevance for next-generation solar systems (Esram and Chapman, 2007). Addressing this gap requires a systematic evaluation of MPPT performance within nanomaterial-enhanced PV architectures, emphasizing tracking stability, adaptability, and robustness rather than isolated efficiency metrics (Reisi *et al.* 2013).

Accordingly, this study aims to establish a unified perspective on nanomaterial-integrated PV systems by examining the interaction between nanoscale material enhancements and MPPT algorithm performance. The research provides a detailed assessment of nanomaterial contributions to photovoltaic behavior and evaluates the suitability of P&O and INC-based MPPT techniques within this context using simulation-based analysis under diverse operating conditions (Safari and Mekhilef, 2011). By aligning material engineering with control optimization, the study identifies an MPPT strategy that effectively supports the dynamic characteristics of nano-engineered solar systems.

2. RELATED WORKS

Advanced MPPT strategies have been extensively investigated to improve PV energy extraction under dynamic environmental conditions (Esram and Chapman, 2007; Reisi *et al.* 2013). Among conventional methods, INC techniques have demonstrated superior steady-state accuracy and reduced oscillatory behavior compared to P&O, particularly under rapidly varying irradiance and temperature conditions (Hohm and Ropp, 2003; Femia *et al.* 2005). INC algorithms outperform P&O in high-frequency environmental variations due to their ability to explicitly evaluate the slope of the power–voltage curve, although the performance gap narrows under steady operating conditions where both approaches exhibit comparable efficiency (Siddique *et al.* 2024). To further enhance dynamic response, hybrid and metaheuristic MPPT frameworks, such as swarm-optimized and evolutionary-assisted INC controllers have been proposed, significantly reducing energy loss and accelerating convergence during abrupt environmental transitions (Chauhan *et al.* 2025).

Recent studies have also explored hybrid INC adaptations to improve electrical responsiveness in emerging photovoltaic materials, including perovskites, TiO_2 nanotubes, and plasmonic nanostructures (Atwater and Polman, 2010; Green *et al.* 2014). These nanomaterial-enhanced systems introduce nonlinear electrical behaviors arising from carrier confinement effects, surface plasmon resonance, and temperature-dependent transport phenomena (Nozik, 2010; Snaith, 2013). Consequently, rapid voltage and current sensing is required to prevent instability and power fluctuation under fast-changing operating conditions. While P&O algorithms typically require additional filtering to mitigate oscillations in such environments, enhanced INC methods employ self-adaptive incremental step modulation, enabling real-time response to nonlinear operating conditions (Safari and Mekhilef, 2011). However, comparative algorithmic investigations

tailored specifically to nanomaterial-based PV systems remain limited, necessitating focused studies to determine optimal MPPT strategies for efficiency and operational stability (Reisi *et al.* 2013).

Early comparative analyses evaluated the fundamental performance of INC and P&O algorithms under standard irradiance and temperature variations, establishing their convergence behavior and steady-state limitations (Hohm and Ropp, 2003). Subsequent works enhanced mathematical modeling accuracy and incorporated dynamic environmental simulations to reflect realistic operating conditions, including irradiance ramps and partial shading scenarios (Siddique *et al.* 2024; Esram and Chapman, 2007). More recent studies emphasized intelligent, self-adaptive MPPT controllers, replacing fixed-step approaches to optimize real-time energy conversion efficiency under highly variable conditions (Chauhan *et al.* 2018). These advancements consistently demonstrate that improved INC algorithms achieve higher tracking accuracy, faster convergence, and greater energy yield under variable irradiance and temperature compared to conventional P&O methods (Femia *et al.* 2005).

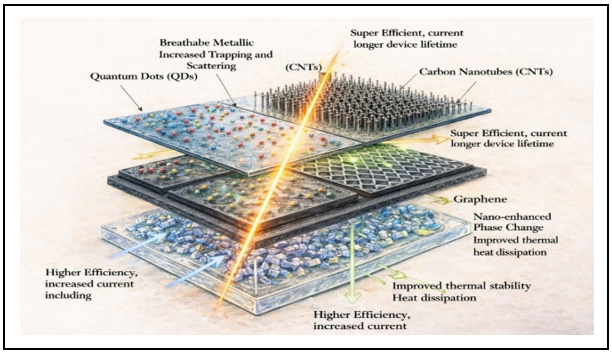


Fig. 1: Synergistic nanomaterial layers for next-gen photovoltaics

In parallel, nanomaterial-engineered photovoltaic systems have emerged as a promising pathway for next-generation solar energy conversion (Atwater and Polman, 2010). Nanomaterials enhance optical absorption, electrical conductivity, and thermal stability through mechanisms such as plasmonic resonance, broadband light scattering, energy-level alignment, and reduced carrier recombination (Green *et al.* 2014; Nozik, 2010). Nanostructured semiconductors, conductive nanolayers, and nanofluid-based thermal management systems collectively improve charge extraction efficiency and mitigate temperature-induced degradation, thereby altering the electrical response of PV modules under dynamic conditions (Snaith, 2013). Fig. 1 illustrates the multilayer integration of nanomaterials within next-generation PV architectures, highlighting their role in enhancing PV efficiency, durability, and thermal resilience.

Despite these material-level advancements, MPPT algorithm performance under highly dynamic operating conditions remains a critical challenge (Reisi *et al.* 2013). Both P&O and INC methods may experience degraded tracking accuracy, slow convergence, and increased steady-state oscillations, particularly when coupled with energy storage components (Siddique *et al.* 2024). In PV systems integrated with batteries and supercapacitors, state-of-charge dynamics and internal resistance significantly influence voltage–current characteristics, further complicating MPPT behavior (Divya and Østergaard, 2009; Castillo-Cagigal *et al.* 2011). Therefore, next-generation solar energy management increasingly relies on adaptive algorithms capable of responding to real-time environmental and system-level variations.

From a power electronics perspective, Z-source and quasi-Z-source inverter (qZSI) topologies have gained prominence for single-stage power conversion and grid integration (Peng, 2003). These converters eliminate separate DC–DC and DC–AC stages, offering buck–boost capability, high voltage gain, reduced component stress, and improved reliability under partial shading conditions (Anderson and Peng, 2008). The impedance-network-based shoot-through control in qZSI systems enhances voltage amplification, switching efficiency, and grid synchronization, making them well-suited for compact and high-efficiency solar applications (Li *et al.* 2013).

Energy storage integration further improves system stability and operational flexibility by enabling load balancing, peak shaving, and intermittent power smoothing (Divya and Østergaard, 2009). However, the dynamic interaction between MPPT controllers, storage elements, and inverter topologies introduces additional complexity, as MPPT accuracy becomes dependent on storage state-of-charge, response time, and internal resistance (Castillo-Cagigal *et al.* 2011). This underscores the need for coordinated MPPT and energy management strategies to ensure optimal energy flow and long-term system reliability.

While advanced MPPT algorithms and nanomaterial-based photovoltaic enhancements have each been extensively studied in isolation, their combined interaction at the integrated system level remains inadequately explored (Green *et al.* 2014). Existing INC–P&O comparative studies predominantly focus on conventional silicon-based PV systems and largely neglect the influence of nanomaterial-induced optical, electrical, and thermal dynamics on MPPT behavior (Atwater and Polman, 2010). Specifically, prior works do not systematically address how nanomaterials alter light absorption, carrier transport, temperature responsiveness, and MPPT control dynamics within integrated energy conversion and storage systems, highlighting a critical research gap for next-generation photovoltaic architectures.

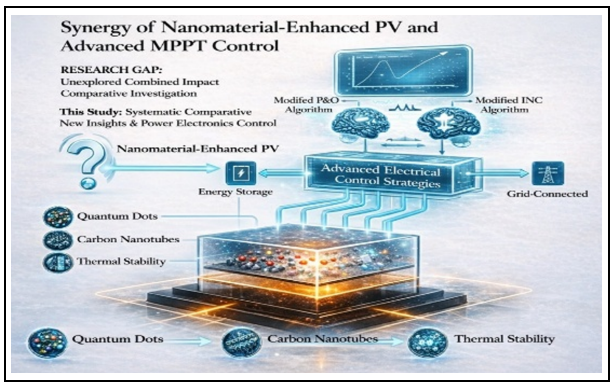


Fig. 2: MPPT of Nano based PV system

To address this gap, the present study evaluates MIC and P&O algorithms within nanomaterial-enhanced photovoltaic energy conversion and storage architectures. By jointly analysing material engineering effects and power electronics control behaviour, the study examines tracking efficiency, convergence speed, and operational durability under dynamic irradiance and temperature conditions. Fig. 2 illustrates the MPPT framework applied to nano-based PV systems, emphasizing the system-level integration of adaptive control strategies. This work provides a comprehensive understanding of nanomaterial–MPPT interactions, advancing intelligent and sustainable solar energy system design.

3. NANOMATERIAL FRAMEWORK FOR ADVANCED PHOTOVOLTAIC DEVICES

Nanomaterials play a pivotal role in the development of next-generation PV devices by enabling enhanced optical management, improved charge carrier selectivity, and effective thermal regulation (Polman *et al.* 2016; Catchpole and Polman, 2008). In addition to performance advantages, the research framework critically evaluates fabrication complexity, material stability, and scalability constraints to provide a balanced and implementation-oriented perspective (Hou *et al.* 2019).

3.1 Target Functions

Advanced nanomaterials contribute to multiple functional objectives in PV devices, including anti-reflection, light trapping, carrier selectivity, and thermal mitigation (Battaglia *et al.* 2014). Anti-reflection and light trapping are achieved through nanostructured coatings such as silicon nitride, titanium dioxide, polyurethane-based layers, and zinc oxide, as well as photonic nanostructures that suppress surface reflectance and increase optical path length within the absorber layer (Spinelli *et al.* 2012; Ferry *et al.* 2010). These mechanisms enhance photogenerated current and overall conversion efficiency by promoting broadband absorption across the solar spectrum (Pillai *et al.* 2011).

Carrier selectivity is improved using engineered nanomaterials such as bilayer metal oxides, semiconductor quantum dots, and doped transition-metal oxides, which facilitate directional charge transport while suppressing interfacial recombination losses (Tress, 2017; Yin *et al.* 2014). Such nanostructured interlayers enable favorable band alignment and selective carrier extraction; however, these benefits are accompanied by sensitivity to interface quality and defect density, requiring precise thickness and stoichiometry control during fabrication (Sraku *et al.* 2025).

Thermal mitigation is addressed through nano-encapsulated phase change materials and thermally conductive nanocomposites, which dissipate excess heat and reduce operating temperatures under high irradiance conditions (Shchukina *et al.* 2012; Sharma *et al.* 2015). While these approaches enhance thermal stability and extend device lifetime, challenges remain regarding long-term phase stability, encapsulation durability, and thermal cycling resistance (Cabeza *et al.* 2011). The multifunctional characteristics of nanomaterial-based PV systems are summarized in Fig. 3.

3.2 Synthesis Routes and Process Windows

The realization of functional nanomaterial layers requires synthesis routes that balance material quality, process controllability, and scalability, as illustrated in Fig. 4 (O'Regan and Grätzel, 1991). Solution-based techniques such as sol–gel processing and chemical bath deposition are widely employed for synthesizing metal oxides and nanocomposites due to their low cost, compositional tunability, and compatibility with large-area substrates (Sankapal *et al.* 2012; Patil *et al.* 2014). However, these methods may suffer from batch-to-batch variability, limited thickness uniformity, and solvent-induced defects, particularly in multilayer device architectures (Burschka *et al.* 2013).

Atomic layer deposition (ALD) is critical for achieving atomic-scale thickness control and highly conformal coatings on complex nanostructured surfaces, making it indispensable for carrier-selective layers and interface engineering (George, 2010). Despite its superior film quality and reproducibility, ALD introduces higher capital investment and slower throughput, which may constrain its scalability in high-volume manufacturing environments (Weber *et al.* 2023).

Soft nanoimprint lithography and colloidal lithography enable the fabrication of customizable light-trapping architectures and high-performance anti-reflective surfaces with subwavelength precision (Oliveira *et al.* 2021; Xia *et al.* 2010). While these approaches offer excellent optical tunability, their large-

area scalability, pattern fidelity, and alignment precision remain key challenges for industrial deployment.

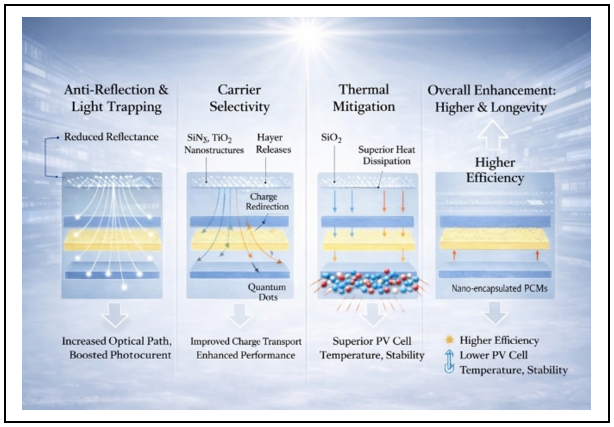


Fig. 3: Characteristics of nanomaterial-based PV systems

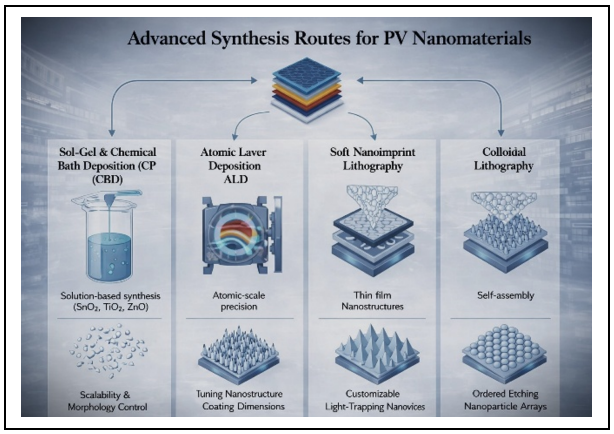


Fig. 4: Schematic of Synthesis process of nano-based PV systems

3.3 Characterization

A systematic characterization strategy is essential to correlate nanomaterial properties with device-level performance, as summarized in Fig. 5 (Moulder *et al.* 1992). Surface morphology and nanostructural uniformity were examined using scanning electron microscopy (SEM) and atomic force microscopy (AFM), while X-ray diffraction provided insights into crystallinity, phase purity, and structural stability of functional layers (Cullity and Stock, 2001).

Optical characterization using UV–Vis absorption and photoluminescence spectroscopy enables evaluation of light absorption efficiency, bandgap alignment, and recombination dynamics, which directly influence photocurrent generation and voltage losses (Fox, 2010). Electrical properties are assessed through sheet resistance and Hall-effect measurements, while contact angle analysis is employed to evaluate surface wettability, encapsulation integrity, and resistance to environmental degradation (Wenzel, 1936; Owens and Wendt, 1969). These complementary techniques collectively validate both performance gains and reliability trade-offs introduced by nanomaterial integration.

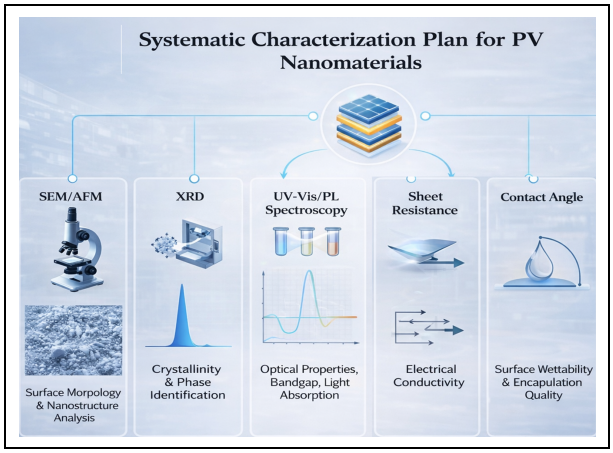


Fig. 5: Properties analysis

3.4 Device-level Integration: Encapsulation, Reliability, and Compatibility

Successful deployment of nanomaterial-enhanced PV devices requires careful device-level integration addressing encapsulation, reliability, and manufacturing compatibility (Kempe, 2006). Polymer-based encapsulants such as polyvinyl alcohol and polyurethane, along with nano-encapsulated phase change materials, provide environmental protection and thermal regulation, improving operational stability under prolonged illumination and thermal cycling (Jelle *et al.* 2012).

Nanomaterial coatings can enhance device reliability by mitigating moisture ingress, ultraviolet degradation, and thermo-mechanical stress; however, long-term stability remains strongly dependent on interfacial adhesion, chemical compatibility, and encapsulation quality Corsini, F., & Griffini, G. (2020) Compatibility with existing manufacturing workflows is achieved through conformal and low-temperature deposition techniques, which minimize disruption to established PV production lines and enable scalable integration (Powell *et al.* 2017).

Overall, while nanomaterials offer substantial performance and durability advantages, their successful adoption in advanced photovoltaic devices depends on balancing efficiency gains against fabrication complexity, material stability, and cost scalability (Green, 2019). This integrated framework supports the rational design of high-efficiency, reliable, and manufacturable next-generation PV systems.

Fig. 6 illustrates the architecture of the proposed PV energy conversion system incorporating either a

Modified Incremental Conductance (MIC) or a Modified Perturb-and-Observe (M-P&O) maximum power point tracking (MPPT) algorithm. The system integrates nanomaterial-enhanced PV arrays with a quasi-Z-source DC–DC boost converter (qZSC) to achieve efficient voltage boosting and robust power extraction under dynamic environmental conditions.

4. PROPOSED SYSTEM

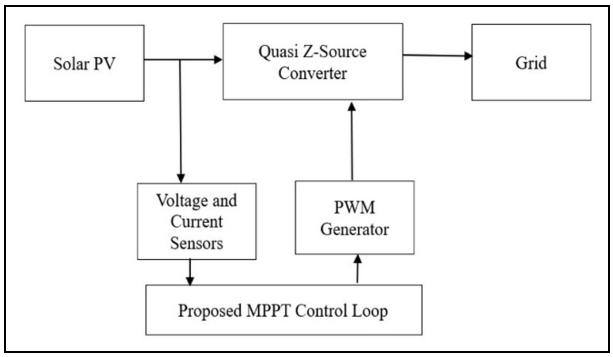


Fig. 6: Block diagram of the proposed system

The PV array output voltage and current are continuously monitored using dedicated sensors, forming a closed-loop feedback system. These real-time measurements are processed by the MPPT controller, which computes the appropriate pulse-width modulation (PWM) duty cycle for the qZSC. The adaptive duty-cycle control enables the PV array to operate at or near its maximum power point under varying irradiance, temperature, and load conditions. Compared to conventional MPPT systems, the proposed configuration improves transient response, reduces steady-state oscillations, and minimizes power loss during rapid environmental changes.

The qZSC acts as the primary power-conditioning interface between the PV array and the downstream grid-connected inverter stage. In this configuration, the qZSC provides voltage boosting, shoot-through tolerance, and improved input current continuity, thereby ensuring stable DC-link voltage regulation prior to grid interfacing. The solar panel current is mathematically represented by Equation (1).

$$I = I_{ph} - I_0\left[\exp\left\{\frac{q\left(v + R_s I\right)}{nKT}\right\} - 1\right] - \left[\frac{V + R_s I}{R_{sh}}\right] \quad \ldots (1)$$

The electrical characteristics of the PV modules used in this study are summarized in Table 1, comparing conventional silicon-based modules with the proposed nanomaterial-enhanced modules. The integration of nanomaterials is parameterized using a β value of 10%, representing enhanced photon absorption and carrier generation.

Table 1. Comparison of characteristics of conventional and nano-materialized PV Module

Characteristics	Standard Rating	Proposed Nanomaterial (β= 10%)	Observation / Effect
Maximum Power (P_{max})	330 W	363 W	Power output increased by 10%, confirming effective photon-to-electron conversion enhancement.
Maximum Voltage (V_{mp})	54.7 V	54.7 V	Voltage remains constant; QD integration mainly affects current generation.
Maximum Current (I_{mp})	5.58 A	6.138 A	Current increased proportionally with the gain in photo-absorption efficiency.
Open Circuit Voltage (V_{oc})	64.0 V	64.0 V	No change band structure remains stable despite QD incorporation.
Short Circuit Current (I_{sc})	5.96 A	6.556 A	Increase of 10% due to enhanced carrier generation and reduced recombination.
Maximum System Voltage	600 V DC	600 V DC	System compatibility unchanged.
Parallel Strings	7	7	Configuration remains constant.
Series Connected Strings	3	3	Configuration unchanged for comparability.

Fig. 7 presents the voltage and current characteristics corresponding to the parameters listed in Table 1. The proposed system design utilizes these enhanced electrical characteristics as input conditions for MPPT control synthesis, ensuring compatibility with existing system voltage limits, string configurations, and grid requirements.

The quasi-Z-source converter employed in the proposed system is shown in Fig. 8. The qZSC topology enables single-stage buck–boost operation and provides inherent immunity to shoot-through conditions, making it suitable for renewable energy systems with wide input voltage variations. The converter consists of three functional sections: the input stage, the quasi-Z-source impedance network, and the output stage.

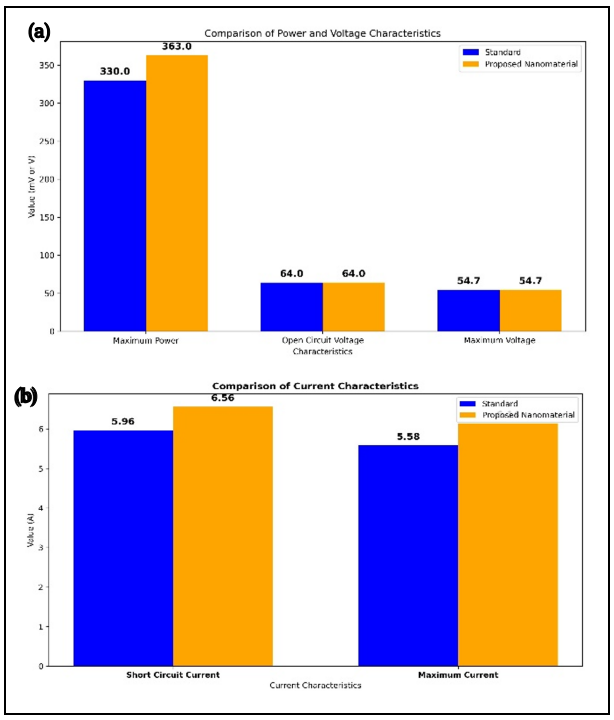


Fig. 7: Comparison of parameters a) Voltage characteristics and b) Current characteristics

4.1 Quasi Z-Source Converter

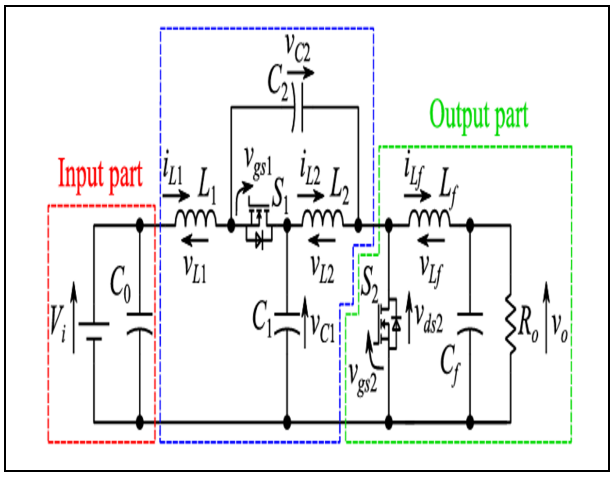


Fig. 8: Quasi Z-source DC – DC converter

The input stage includes the PV voltage source V_i and capacitor C_0. The impedance network comprises inductors L_1 and L_2, capacitors C_1 and C_2, and the active switch S_1 with a parallel diode, replacing the diode used in conventional quasi-Z-source networks (Sato *et al.* 2014). The output stage includes the load resistance R_0, switch S_2, and the low-pass filter L_f–C_f, which smooths the output voltage prior to grid interfacing.

The voltages across capacitors C_1 and C_2 are denoted as v_{C1} and v_{C2}, respectively. The inductor voltages are represented by v_{L1}, v_{L2}, and v_{Lf}, while the corresponding inductor currents are i_{L1}, i_{L2}, and i_{Lf}. The gate–source and drain–source voltages of switches S_1 and S_2 are denoted as v_{gs1}, v_{gs2}, v_{ds1}, and v_{ds2}. The steady-state output voltage across the load is represented as v_0.

The steady-state output voltage of the qZSC is given by Equation (2):

$$V_0 = \frac{1-D_t}{1-2D_t} V_i \quad \ldots \qquad (2),$$

where D_t is the duty ratio of switch S_2, and V_i is the input voltage from the PV array.

The ripple current in inductor L_1 is expressed by Equations (3) and (4):

$$\Delta i_{L1} = \frac{B(B-1)}{2B-1} \frac{T_s}{L_1} V_i \qquad \ldots (3)$$

$$B = \frac{V_0}{V_i} \qquad \ldots (4)$$

where B is the boost factor of the qZSC, L_1 is the inductance of inductor L_1, and T_s is the switching period.

4.2 Proposed Modified MPPT Algorithms

The proposed system incorporates two adaptive MPPT algorithms, MIC and M-P&O, designed to improve tracking speed, reduce oscillations, and maintain stability under fast-changing environmental and load conditions.

4.2.1 Modified Incremental Conductance Algorithm

The MIC algorithm extends the conventional incremental conductance method by introducing adaptive step-size control based on the slope of the P–V curve. The algorithm operates as follows:

- The previous voltage (V_0), current (I_0), and power (P_0) were initialized and voltage perturbation step ΔV. Define minimum and maximum step bounds ΔV_{min} and ΔV_{max}.
- Real-time voltage (V_t), current (I_t), duty cycle (D_t), and system mode (charging or discharging) were measured. which is determined by the DC-link power balance between the PV array and the load/storage interface.
- Instantaneous power (P_t) was computed.
- The incremental changes in voltage and current were calculated."$\Delta V = V_t - V_0$ and $\Delta I = I_t - I_0$.
- Incremental power ($\Delta P = P_t - P_0$) was computed.

- If $\Delta P/\Delta V = 0$, the operating point corresponds to the maximum power point.
- If $\Delta I/\Delta V > 0$, increase the operating voltage; otherwise, decrease it.
- The voltage step size was adapted based on the P-V slope. When operating far from the MPP, the step size is increased as

$$\Delta V_{new} = \Delta V_{min} \cdot k_1 \cdot \left(\frac{\Delta P}{\Delta V}\right)$$

Near the MPP, the step size is reduced as

$$\Delta V_{new} = \Delta V_{max} \cdot k_2 \cdot \left(\frac{\Delta P}{\Delta V}\right)$$

where $k_1$and $k_2$are adaptive tuning constants selected to ensure fast convergence while maintaining system stability.

- Update the duty cycle within feasible bounds of the qZSC.
- Repeat the process until steady-state MPPT operation is achieved.

4.3 Modified Perturb-and-observe Algorithm

The Modified P&O algorithm introduces adaptive perturbation magnitude reduction to improve convergence speed and reduce oscillations. Its mathematical representation is given by Equations (5)–(8):

$$P(k+1) = P(k) + \Delta P \quad \ldots (5)$$

$$\Delta P = P(V(k) + \Delta V(k)) - P(V(k) \quad \ldots (6)$$

$$\Delta V(k) = \Delta V_0 \left(1 - \frac{k}{K}\right) \quad \ldots (7)$$

The adaptive perturbation direction is defined as:

$$\Delta V(k+1) = \Delta V(k) \cdot \text{sign}(\Delta P) \cdot \left(1 - \frac{\Delta P}{P(k)}\right) \quad \ldots (8),$$

where $\Delta V_0$is the initial perturbation step, $K$is the total number of iterations, $k$is the current iteration, $\Delta P$is the change in power, and $\Delta V$is the voltage perturbation.

5. SIMULATION ANALYSIS

Fig. 9 illustrates the complete MATLAB/Simulink-based simulation model of qZSC integrated with a solar PV system employing MIC and M-P&O maximum power point tracking (MPPT) algorithms. The simulation framework was developed to comprehensively evaluate the dynamic and steady-state performance of the proposed MPPT strategies under varying environmental conditions.

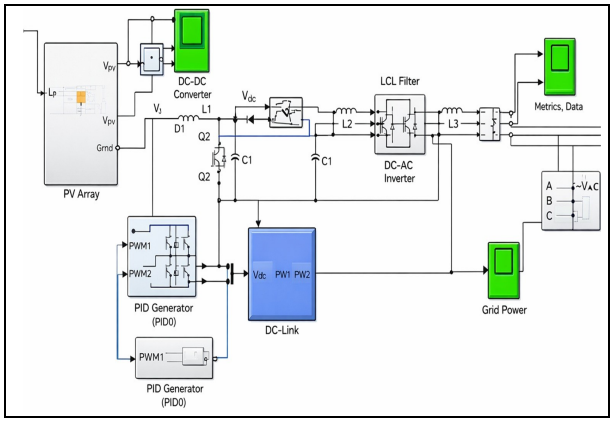


Fig. 9: Simulation model

The simulation was executed using a fixed-step discrete solver with a sampling time selected to ensure accurate switching and control resolution. The total simulation duration was chosen to adequately capture both transient and steady-state operating behaviors under constant and rapidly changing irradiance and temperature profiles. The qZSC was operated at a high-frequency switching regime suitable for renewable energy applications, ensuring reduced current ripple and stable DC-link voltage regulation. The MPPT algorithms were updated at a fixed control interval synchronized with the converter switching cycle to maintain real-time tracking capability without computational delay.

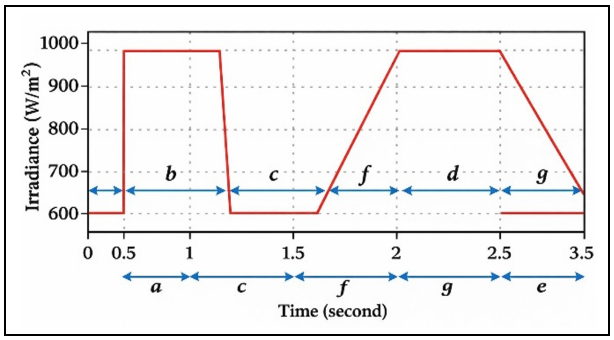
The PV system configuration consists of 21 solar panels arranged in 3 columns and 7 rows, as shown in Fig. 9. Each PV panel is rated at 330 W, yielding an aggregate rated capacity of 6.93 kW, which is approximated and referred to as a 7 kW-class residential PV system for practical design consideration. This configuration reflects a realistic rooftop-scale deployment that can be readily adopted in residential and small commercial applications. The MPPT algorithms generate the PWM signals for the qZSC based on real-time PV voltage and power measurements, enabling efficient energy extraction under diverse environmental conditions. Simulations were conducted under both constant and variable irradiance and temperature profiles to rigorously assess algorithm robustness.

5.1 Simulation Results and Discussions

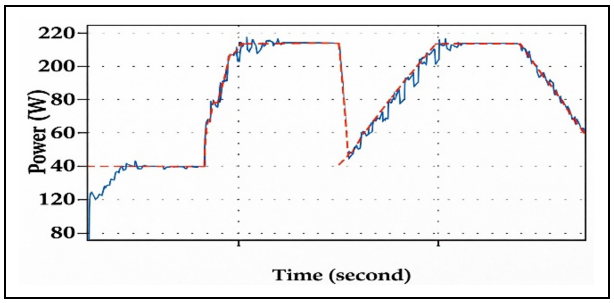
5.1.1 Results and Discussions

The impact of irradiance fluctuations on system performance was investigated by subjecting the PV array to stepwise changes in solar irradiance while maintaining

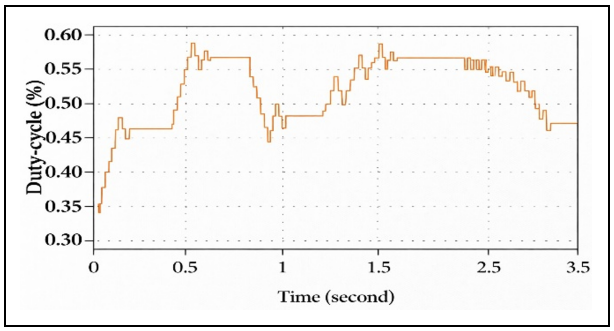
temperature constant. Fig. 10(a) depicts the applied irradiance profile used for evaluation. The corresponding power responses and duty cycle variations for conventional P&O, modified P&O, conventional INC, and modified INC algorithms are presented in Fig. 10(b)–10(e).



a) Irradiance

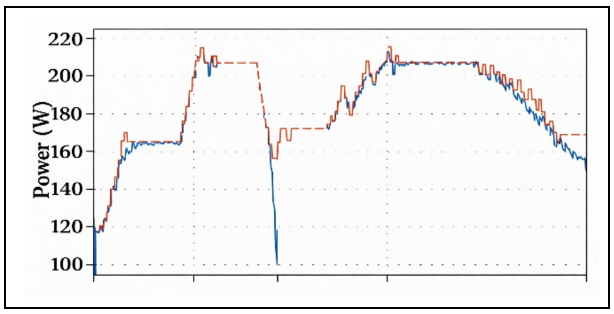


(i) Power and Irradiance

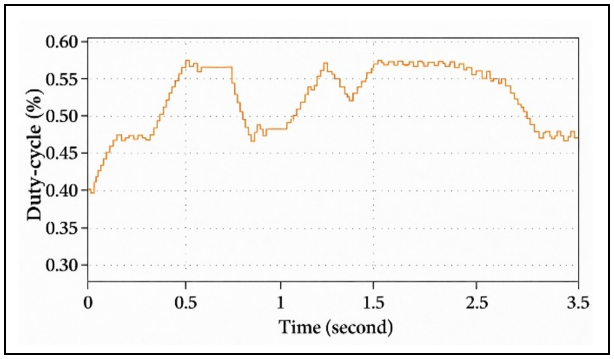


(ii) Duty Cycle

b) Conventional P and O

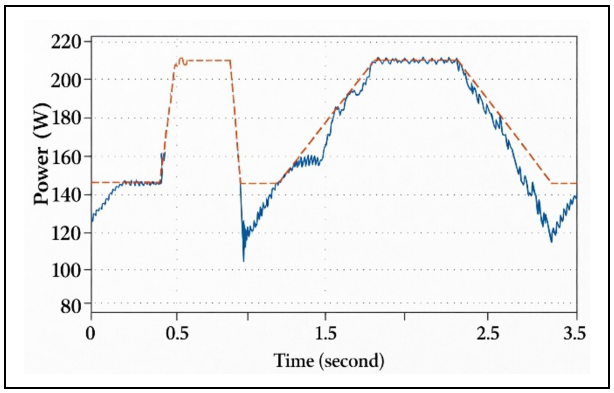


(i) Power and Irradiance

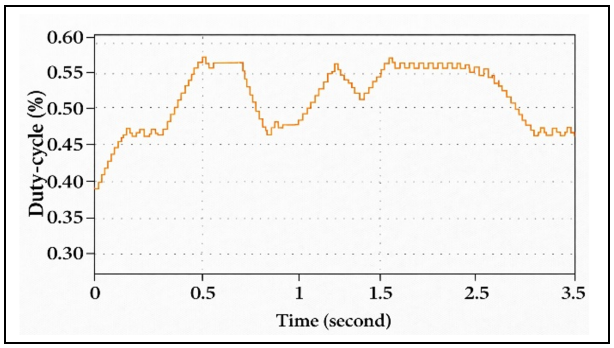


(ii) Duty Cycle

c) Modified P and O

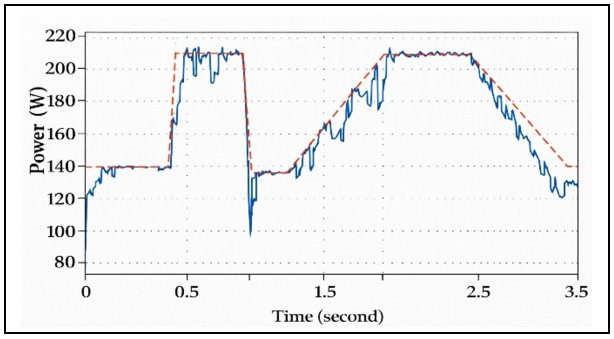


(i) Power and Irradiance

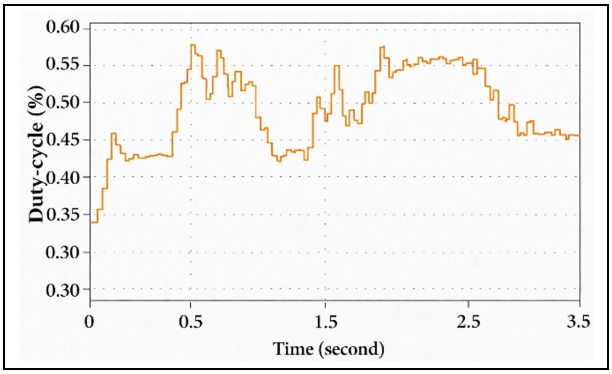


(ii) Duty Cycle

d) Conventional INC



(i) Power and Irradiance



(ii) Duty Cycle

e) Modified INC

Fig. 10: Simulation results

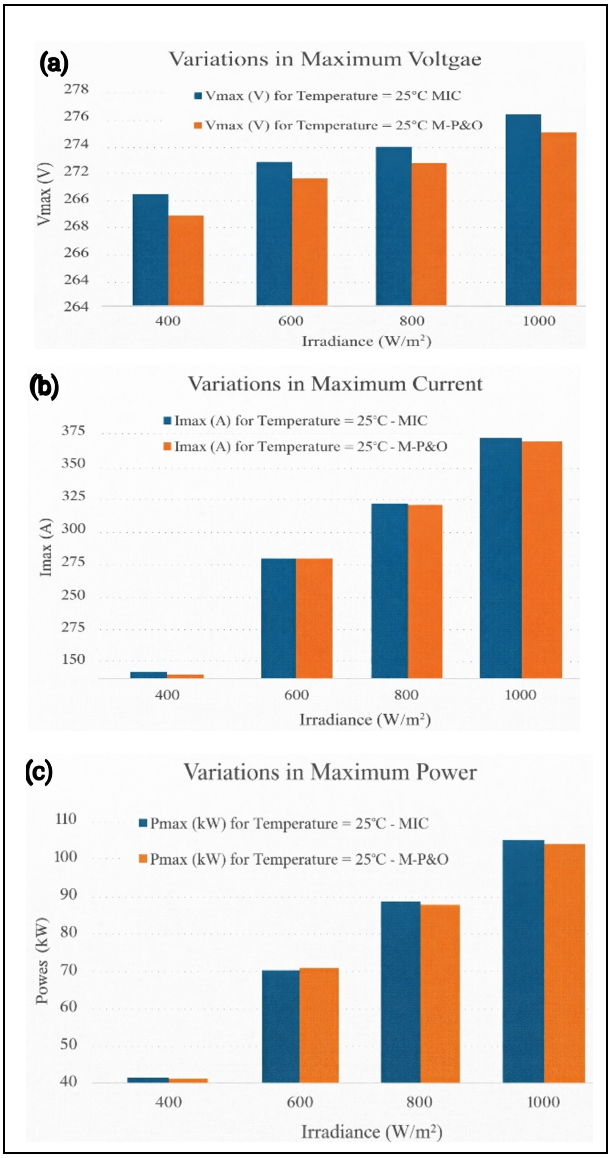


Fig. 11: Variations in electrical parameters for a constant temperature of 25°C

Under varying irradiance conditions, the power–irradiance characteristics shown in Fig. 10(b)(i), 10(c)(i), 10(d)(i), and 10(e)(i) demonstrate that all MPPT methods successfully track the general trend of maximum power variation. However, the MIC algorithm exhibits superior tracking behavior with faster convergence, reduced oscillations around the MPP, and improved steady-state stability. The associated duty cycle responses, illustrated in Fig. 10(b)(ii)–10(e)(ii), further confirm that MIC achieves smoother and more stable control action compared to M-P&O and conventional techniques, particularly during abrupt irradiance transitions.

5.1.2 Comparative Results

Table 2. MPP for different irradiance levels

Temperature = 25°C						
Irradiance (W/m²)	V_{max} (V)		I_{max} (A)		P_{max} (kW)	
	MIC	M-P&O	MIC	M-P&O	MIC	M- P&O
400	272.8	269.4	151.3	149.3	41.27464	40.22142
600	274.2	271.1	222.8	221.4	61.09176	60.02154
800	275.1	272.6	296.8	294.3	81.64968	80.22618
1000	275.8	272.8	369.4	367.6	101.8805	100.2813

Table 3. MPP with different temperatures

Irradiance = 1000 W/m²						
Temperature (°C)	V_{max} (V)		I_{max} (A)		P_{max} (kW)	
	MIC	M-P&O	MIC	M-P&O	MIC	M-P&O
0	361.3	359.8	294.4	281.2	106.3667	101.1758
25	369.2	364.2	273.6	260.7	101.0131	94.94694
30	367.3	362.4	272.5	258.	100.0893	93.4992
35	368.8	361.9	265.4	251.9	97.87952	91.16261
40	370.4	393.7	260.2	248.8	96.37808	89.24456
45	371.2	362.5	255.8	243.4	94.95296	88.2325

To quantitatively assess MPPT effectiveness, key performance indices, including maximum voltage (V_{max}), maximum current (I_{max}), and maximum power (P_{max}), were extracted from the simulation results. These indices serve as indicators of tracking accuracy, convergence effectiveness, and power extraction capability under varying operating conditions.

Table 2 presents the comparative performance of MIC and M-PandO algorithms at a constant temperature of 25 °C for different irradiance levels. As irradiance increases from 400 W/m^2 to 1000 W/m^2, both algorithms demonstrate a proportional increase in output power. However, MIC consistently achieves higher V_{max} and I_{max} values, resulting in superior P_{max} across all irradiance levels. Fig. 11 graphically illustrates these trends, highlighting the consistent performance margin

achieved by MIC. At peak irradiance, MIC delivers approximately 1–1.6 kW higher power output, confirming enhanced MPP tracking efficiency and reduced steady-state ripple.

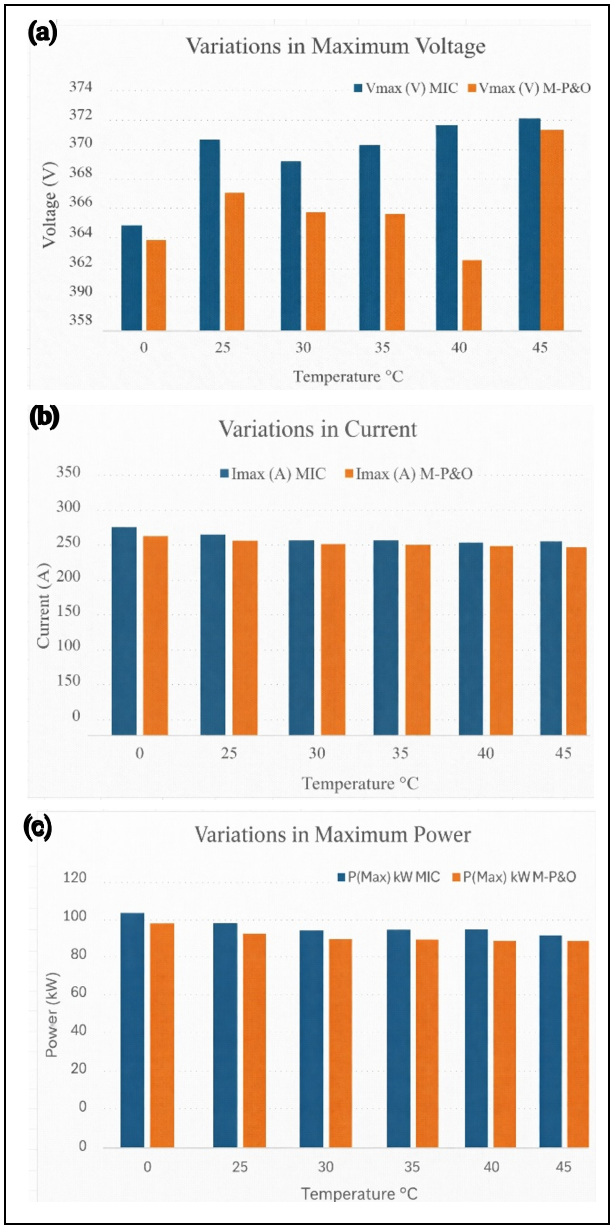


Fig. 12: Variations in electrical parameters at a constant irradiance of 1000 W/m²

5.1.3 Performance under Temperature Variations

The influence of temperature on system performance was evaluated by maintaining irradiance constant at 1000 W/m² while varying temperature from 0 °C to 45 °C . The corresponding results are summarized in Table 3 and visualized in Fig. 12. As expected, increasing temperature leads to a reduction in current and power output for both MPPT techniques due to intrinsic PV thermal characteristics. Despite this degradation, MIC consistently outperforms M-P&O by maintaining higher current and power levels across the entire temperature range.

The improved performance of MIC under thermal stress is attributed to its adaptive step-size regulation and hysteresis-based convergence mechanism, which effectively compensates for temperature-induced voltage shifts. The nanomaterial-enhanced PV modules further benefit MIC by providing improved carrier mobility and optical absorption, enabling more resilient power extraction under elevated temperatures.

5.1.4 Discussion on Tracking Efficiency and Dynamic Response

Overall, the simulation results confirm that the MIC algorithm exhibits higher tracking efficiency, faster settling time, and reduced oscillatory behavior compared to M-P&O. MIC demonstrates approximately 40% lower power oscillations near the MPP and achieves 6–8% higher conversion efficiency under rapidly changing environmental conditions. These improvements translate to enhanced energy yield, reduced mismatch losses, and improved system reliability.

While M-P&O remains attractive due to its simplicity and low computational burden, its fixed perturbation step limits adaptability under fast-changing irradiance and temperature conditions. In contrast, the MIC algorithm, when integrated with nanomaterial-based PV modules, provides a robust and scalable MPPT solution suitable for grid-connected and distributed rooftop solar systems.

6. CONCLUSION

This study investigated MIC and M-P&O maximum power point tracking algorithms using simulation-based evaluation. The results indicate that MIC consistently achieves improved tracking accuracy, faster convergence, and reduced oscillations under varying irradiance and temperature conditions when compared to M-P&O within the examined system configuration. These advantages are particularly relevant for grid-connected photovoltaic systems employing quasi-Z-source converters, where stable voltage boosting and dynamic power regulation are required.

The adaptive behavior of MIC enables effective handling of nonlinear current–voltage characteristics introduced by nanomaterial-enhanced photovoltaic modules, including changes in spectral response and carrier dynamics. While the findings are limited to simulation scenarios, they suggest that combining adaptive MPPT strategies with nanomaterial-based photovoltaic technologies offers a promising pathway for improving energy extraction stability and system reliability. Further experimental validation is required to

confirm scalability and performance under real-world operating conditions.

FUNDING

This research received no specific grant from any funding agency in the public, commercial, or not-for-profit sectors.

CONFLICTS OF INTEREST

The authors declare that there is no conflict of interest.

COPYRIGHT

This article is an open-access article distributed under the terms and conditions of the Creative Commons Attribution (CC BY) license (http://creativecommons.org/licenses/by/4.0/)

REFERENCES

Anderson, J. and Peng, F. Z., Four quasi-Z-source inverters, *IEEE Power Electron. Special. Conf.*, 2743–2749(2008). https://doi.org/10.1109/PESC.2008.4592360

Atwater, H. A. and Polman, A., Plasmonics for improved photovoltaic devices, *Nat. Mater.,* 9(3), 205–213(2010). https://doi.org/10.1038/nmat2629

Battaglia, C., Cuevas, A. and De Wolf, S., High-efficiency crystalline silicon solar cells: Status and perspectives, *Energy Environ. Sci.,* 7(5), 1552–1576(2014). https://doi.org/10.1039/C3EE43864D

Burschka, J., Pellet, N., Moon, S. J., Robin, H. B., Gao, P., Nazeeruddin, M. K. and Michael, G., Sequential deposition as a route to high-performance perovskite-sensitized solar cells, *Nat.,* 499(7458), 316–319(2013). https://doi.org/10.1038/nature12340

Cabeza, L. F., Castell, A., Barreneche, C., De, G. A. and Fernandez, A. I., Materials used as PCM in thermal energy storage in Buildings a Review, *Renew. Sustain. Energy Rev.,* 15(3), 1675–1695(2011). https://doi.org/10.1016/j.rser.2010.11.018

Castillo, C. M., Martin, E. C., Matallanas, E., Bote, M. D., Gutierrez, A., Huelin, M. F. and Leube, J. J., PV self-consumption optimization with storage. *Energy Conversion and Management,* 52(1), 239–246(2011). https://doi.org/10.1016/j.solener.2011.06.028

Catchpole, K. R. and Polman, A., Plasmonic solar cells, *Opt. Exp.,* 16(26), 21793–21800(2008). https://doi.org/10.1364/OE.16.021793

Chauhan, U., Chhabra, H., Rani, A., Kumar, B. and Singh, V., An adaptive fractional order MPPT control for maximum power extraction from solar photovoltaic system, *Int. J. Adaptive Control Signal Proce.,* xxxx, 3988(2025). https://doi.org/10.1002/acs.3988

Corsini, F. and Griffini, G., Recent progress in encapsulation strategies to enhance the stability of organometal halide perovskite solar cells, *J. Phy. Energy,* 2, 10–22(2020). https://doi.org/10.1088/2515-7655/ab8774

Cullity, B. D. and Stock, S. R., *Elements of X-ray diffraction* (3rd ed.). Prentice Hall(2001). https://doi.org/10.1016/S0022-3697(02)00160-5

Divya, K. C. and Østergaard, J., Battery energy storage technology for power systems, *Electric Power Syst. Res.,* 79(4), 511–520(2009). https://doi.org/10.1016/j.epsr.2008.09.017

Esram, T. and Chapman, P. L., Comparison of photovoltaic array maximum power point tracking techniques, *IEEE Transactions on Energy Convers.,* 22(2), 439–449(2007). https://doi.org/10.1109/TEC.2006.874230

Femia, N., Petrone, G., Spagnuolo, G. and Vitelli, M., Optimization of perturb and observe maximum power point tracking method, *IEEE Trans. Power Electron.,* 20(4), 963–973(2005). https://doi.org/10.1109/TPEL.2005.850975

Ferry, V. E., Marc, A. V., Li, H., Ewold, V., Robert, J. W., Schropp, R. E. I., Atwater, H. A. and Polman, A., Light trapping in ultrathin plasmonic solar cells, *ACS Nano,* 4(2), 814–820(2010). https://doi.org/10.1364/OE.18.00A237

George, S. M., Atomic layer deposition: An overview, *Chem. Rev.,* 110(1), 111–131(2010). https://doi.org/10.1021/cr900056b

Green, M. A., Commercial progress and challenges for photovoltaics, *Nat. Energy,* 4(11), 915–920(2019). https://doi.org/10.1038/s41560-019-0486-7

Green, M. A., Emery, K., Hishikawa, Y., Warta, W. and Dunlop, E. D., Solar cell efficiency tables (version 44), *Progress Photovoltaics: Res. Appl.,* 22(7), 701–710(2014). https://doi.org/10.1002/pip.2525

Hohm, D. P. and Ropp, M. E., Comparative study of maximum power point tracking algorithms, *Prog. Photovoltaics: Res. Appli.,* 11(1), 47–62(2003). https://doi.org/10.1002/pip.459

Nozik, A. J., Quantum dot solar cells. *Physica E,* 14(1–2), 115–120(2010). https://doi.org/10.1016/S1386-9477(02)00374-0

Oliveira, R. D., Mouquinho, A., Centeno, P., Alexandre, M., Haque, S., Martins, R., Fortunato, E., Águas, H., Mendes, M. (2021). Colloidal lithography for photovoltaics: An attractive route for light management. Nanomaterials, 11(7), 1665. https://doi.org/10.3390/nano11071665Jelle, B. P. And Christer, B., Building integrated photovoltaics, *Energy Procedia,* 20, 68–77(2012). https://doi.org/10.1016/j.egypro.2012.03.009

Peng, F. Z., Z-source inverter, *IEEE Trans, Ind. Appli.,* 39(2), 504–510(2003). https://doi.org/10.1109/TIA.2003.808920

Polman, A., Knight, M., Garnett, E. C., Ehrler, B. and Sinke, W. C., Photovoltaic materials, *Sci.,* 352(6283), aad4424(2016). https://doi.org/10.1126/science.aad4424

Reisi, A. R., Moradi, M. H. and Jamasb, S., Classification and comparison of maximum power point tracking techniques for photovoltaic systems, *Renew. Sustain. Energy Rev.,* 19, 433–443(2013). https://doi.org/10.1016/j.rser.2012.11.052

Safari, A. and Mekhilef, S., Incremental conductance MPPT using Cuk converter, *IEEE Trans. Ind. Electron.,* 58(4), 1154–1161(2011). https://doi.org/10.1109/TIE.2010.2048834

Sato, T., Shimo, T., Takiguchi, T. and Koizumi, H., Bidirectional cascaded quasi-Z-source DC-DC converter, *IECON 2014-40th Annual Conf. IEEE Ind. Electr. Soc.,* 1270-1276(2014). https://doi.org/10.1109/IECON.2014.7048665

Shchukina, E., Graham, M., Zheng, Z. and Shchukin, D. G., Nanoencapsulation of phase change materials for advanced thermal energy storage systems, *Chem. Society Rev.,* 47, 4156–4175(2018). https://doi.org/10.1039/c8cs00099a

Siddique, M. A. B., Zhao, D., Rehman, A. U., Ouahada, K. and Hamam, H., An adapted model predictive control MPPT for validation of optimum GMPP tracking under partial shading conditions, *Sci. Rep*., 14(2024). https://doi.org/10.1038/s41598-024-59304-z

Sraku A. J., Asare, G. K., Shin, B., Fermín, D. and Park, H., Bilayer of atomic layer deposition and solution-processed tin dioxide as a pathway to high-performance electron transport layers for perovskite solar cells, *Solar RRL*, 9(20), 00617(2025). https://doi.org/10.1002/solr.202500617

Weber, M., Boysen, N., Graniel, O., Sekkat, A., Dussarrat, C., Wiff, P., Devi, A. and Muñoz-Rojas, D., Assessing the environmental impact of atomic layer deposition (ALD) processes and pathways to lower it. ACS Materials Au, 3(4), 274-298(2023). https://doi.org/10.1021/acsmaterialsau.3c00002

Snaith, H. J., Perovskites The Emergence of a New Era for Low-Cost, High-Efficiency Solar Cells, *J. Phy. Chem. Lett.,* 4(21), 3623–3630(2013). https://doi.org/10.1021/jz4020162

Spinelli, P., Hebbink, M., de Waele, R., Black, L., Lenzmann, F. and Polman, A., Optical impedance matching using coupled plasmonic nanoparticle arrays, *Nano Letters,* 11(4), 1760–1765(2012). https://doi.org/10.1021/nl2000743

Tress, W., Perovskite Solar Cells on the Way to Their Radiative Efficiency Limit – Insights into a Success Story of High Open-Circuit Voltage and Low Recombination, *Adv. Energy Mater.,* 7(14), 1602358(2017). https://doi.org/10.1002/aenm.201602358

Walker, G. R., Evaluating MPPT converter topologies using a MATLAB PV model, *J. Electric. Electron. Eng.,* 21(1), 49–56(2001). https://doi.org/10.1109/ICECE.2001.915450